A precise characterization of three-dimensional percolating backbones

1994 J. Phys. A: Math. Gen. 27 5445

(http://iopscience.iop.org/0305-4470/27/16/011)

J. Phys. A: Math. Gen. 27 (1994) 5445–5454. Printed in the UK

A precise characterization of three-dimensional percolating backbones

M D Rintoul and Hisao Nakanishi

Department of Physics, Purdue University, W Lafayette, IN 47907, USA

Received 23 February 1994, in final form 24 May 1994

Abstract. The backbones of three-dimensional critical percolation clusters are extracted and the fractal dimension is accurately calculated using various mass-scaling and box-counting techniques to be $d_f^B = 1.855 \pm 0.015$. The eigenvalue spectrum of the Brownian transition probability matrix is studied numerically, which results in the estimates $d_w^B = 3.13 \pm 0.03$ for the walk dimension and $d_s^B = 1.18 \pm 0.01$ for the spectral dimension of the backbone. Independent calculation of all three quantities allows the conductivity exponent $\tilde{\mu}$ to be determined and also allows the validity of the scaling relation $d_s = 2d_f/d_w$ proposed by Alexander and Orbach to be tested on the backbone.

1. Introduction

The backbone part of the percolating cluster has been studied almost as widely as the full percolation cluster itself. This is due to the fact that the multi-connectedness of the sites plays a vital role in many of the physical processes that are studied on the percolation cluster. These processes include gel structure [1, 2], fluid flow in porous media [3], and especially random resistor networks [4–6]. Other new and interesting applications include the distribution of earthquake hypocentres [7]. The backbone is also interesting for purely theoretical reasons. It is another example of a homogeneous fractal which can be used for testing various scaling relationships between different critical exponents. There are phenomena which are not constrained to the backbone and yet whose properties are dominated by those of the backbone.

One of the more intersting cases is the random walk. A random walk on a critically disordered medium may exhibit a behaviour known as *anomalous diffusion*, where the relationship between the mean-square displacement and the time is no longer Fickian. Instead, the particle is slowed down by the disorder in the system and the diffusion law becomes

$$\langle R^2(t) \rangle \sim t^{2/d_w} \tag{1}$$

where the walk dimension $d_w > 2$ [8]. The increase in the walk dimension due to anomalous diffusion is not only relevant to random walks, but to the problem of conduction in a disordered medium. The conductivity exponent of a disordered system $\tilde{\mu}$, which is defined by $\sigma_{dc}(R) \sim R^{-\tilde{\mu}}$, where R describes the length scale of the system, can be related to the walk dimension of the medium via the Einstein relation

$$\sigma_{dc} = \frac{e^2 n}{k_B T} D \tag{2}$$

0305-4470/94/165445+10$19.50

where e is the carrier charge, n is the carrier density, and D is the diffusion constant. Using the fact that $D \sim R^2/t$ and $n \sim R^{d_f-d}$, along with (1), we obtain

$$d_w = 2 - d + d_f + \tilde{\mu} \tag{3}$$

where d_f is the fractal dimension of the disordered medium. However, on a percolation cluster, all of the current is carried by the backbone sites, so the above relationship can be rewritten as [3]

$$d_w^B = 2 - d + d_f^B + \tilde{\mu} \tag{4}$$

where the fractal exponents now refer to the backbone and $\tilde{\mu}$ remains the same. One can often calculate the conductivity exponent much more efficiently using (4) since no effort is wasted on the dangling ends of the full cluster.

Another important exponent describing the fractal medium is the *spectral* (or *fracton*) dimension d_s. This exponent describes the vibrational density of states in the medium as given by the relationship

$$N(\omega) \sim \omega^{d_s-1} \tag{5}$$

where ω is the vibrational frequency, in the low-energy region. Relating the density-of-states problem to that of the return to the origin problem, Alexander and Orbach derived the scaling relation [9]

$$d_s = \frac{2d_f}{d_w}. \tag{6}$$

Recent work by Dhar and Ramaswamy [10], which was later confirmed by Nakanishi and Herrmann [11], has shown that this conjecture may not hold on some loopless structures such as Eden trees. Their argument is that all of the sites are not sampled uniformly but instead the walker gets trapped on a specific branch of the tree. Therefore one of the assumptions that go into the Alexander–Orbach scaling relation (equation (6)) does not hold. For percolation backbones, one would expect that the multi-connectedness of the sites assures that the occupation probabilities would be much more uniform, and that (6) should hold.

In order to evaluate d_w^B and d_s^B, we use a method based on the transition probability matrix associated with the random walk on the cluster S. The random walk on S has associated with it a transition probability matrix W where the entries W_{ij} are just the probability for a random walker at site j to jump to site i in a given time-step. This implies that W will be an $s \times s$ Markov matrix, where s is the number of sites in cluster S. The Markov property of W is assured since the transition probabilities for a single site (and therefore a single column of W) must sum to 1 and will also be non-negative. All of the properties of a random walk on S should be available through the various properties of W.

To extract d_s^B from W, we note that for the eigenvalues λ of W near 1, the density of eigenvalues $n(\lambda)$ should scale as [12]

$$n(\lambda) \sim |\ln \lambda|^{d_s^B/2-1} \tag{7}$$

where $|\ln \lambda|$ plays the role of ω^2 which appears in (5). In order to extract d_w^B from W, we must first look at the function [13]

$$\pi(\lambda) = n(\lambda) a_\lambda (\lambda - 1)^2 \tag{8}$$

where the a_λ are just the coefficients from the position autocorrelation function

$$\langle r(t) \cdot r(0) \rangle = \sum_\lambda a_\lambda \lambda^t \tag{9}$$

and are determined by expanding the initial distribution of the random walk in terms of the eigenvectors of W. This function should scale, for large λ, as [14]

$$\pi(\lambda) \sim |\ln \lambda|^{1-2/d_w^B} . \tag{10}$$

In order to calculate the conductivity or test the scaling relation due to Alexander and Orbach, it is also necessary to know the *fractal* dimension of the system. One of the most accurate ways of determining the fractal dimension of an object constructed on lattices of varying size is through so-called mass scaling. The mass (or the number of sites) of a percolating cluster backbone constructed between two opposite faces on an L^3 grid should scale as

$$M(L) \sim L^{d_f^B} . \tag{11}$$

The slope of a log–log plot of the backbone cluster mass as a function of the grid size should therefore yield an estimate of d_f^B. This method has been used widely to estimate the fractal dimension of the backbones and other geometrical objects [16–18]. It was previously used in [15] to obtain the fractal dimension of the two-dimensional backbones.

Additionally, one can calculate a whole spectrum of fractal dimensions $D_f(q)$ in the following manner [19]:

$$D_f(q) = \lim_{\epsilon \to 0} \frac{1}{q-1} \frac{\ln \sum_{\nu=1}^{N(\epsilon)} [p_\nu(\epsilon)]^q}{\ln \epsilon} \tag{12}$$

where ν labels the boxes and

$$p_\nu(\epsilon) = \frac{N_\nu(\epsilon)}{N} \tag{13}$$

is the fraction of total points falling in box ν of linear size ϵ. For $q = 0$, this just corresponds to the traditional box-counting definition of the fractal dimension. This method was most widely used for multi-fractal analysis [20–22], and is especially suited for fractals with self similarity extending to arbitrarily short length scales. For simple fractal objects (objects which are not *multifractals*), all of the $D_f(q)$ should be equal and would therefore all correspond to d_f^B in our case.

2. Numerical methods

The percolation clusters were generated by assigning every site on a simple cubic grid of size L^3 to be either occupied with probability p, where $p = 0.3117 \approx p_c$, or unoccupied otherwise. The largest connected cluster on the grid was then identified and checked to see if it spanned the entire length of the grid in at least one direction. If it did not, it was rejected and the sites of the grid were assigned again. If it did span in at least one direction, two points on opposite faces were chosen and the backbone defined between those two points was extracted by means of a burning algorithm [17].

Mass-scaling calculations were done on these L^3 grids, where $4 \leqslant L \leqslant 300$. For the range $L \leqslant 100$, the number of clusters averaged over to calculate the mass was $10^7/L^2$. For $L \geqslant 100$, the number of clusters used was 500. This allowed us to get a sufficient number of data points for large L and to see if there were any finite-size effects for smaller L, while still obtaining reasonable accuracy for a given L.

The box counting was done using the method described by Liebovitch and Toth [23] with the modification of cyclic bit ordering as described in detail in [24]. A value of $L = 512$ was used in order to get as many factors of two as possible in box size, as our resolution was ultimately limited by the lattice spacing. This large value of L required us

Table 1. Total number and average size of the clusters used in the calculation of d_w^B and d_s^B.

L	Samples	Cluster size	BB size
70	1400	10 774	1306
100	917	27 728	2689
150	898	72 202	5379

to use a bit-based algorithm to generate the clusters and extract the backbone. Each site on the cluster was allocated a total of two bits of memory. This allowed the site to be in a total of four different states, which was enough to carry out the cluster creation, largest cluster extraction, and burning algorithm in a practical manner. The computer memory was allocated dynamically during the construction of each cluster and released after a compressed list of points describing the backbone was created. This allowed us to run the $L = 512$ cases using the amount of memory on readily available computers and not supercomputers, which were not necessarily as accessible.

Although the value for $D_f(q)$ described in (12) is obtained in the $\epsilon \to 0$ limit, in practice the value must be estimated from a linear fit to a range of ϵ which is determined by inspection of the data [23]. This is because our fractal has a small length cut-off, and as ϵ becomes approximately equal to the lattice spacing, the equation no longer makes sense. The values for large ϵ also cannot be used since they are not adequately measuring the fractal nature of the cluster. For our values of q, values of ϵ were chosen in the region $2 \leqslant \epsilon \leqslant 128$.

The eigenvalue and eigenvector coefficient extraction was done using a variation of the Lanczos method which is useful for large, sparse matrices as described in [14]. The specific algorithm used was first proposed by Arnoldi in [25] and later expanded on by Saad [29], and then adapted for diffusion problems in [14]. In this method, a subspace of the domain of the original matrix corresponding to the largest eigenvalues is approximately extracted, and then the corresponding submatrix is exactly diagonalized to extract the eigenvalues and eigenvectors. This method has proven itself to be very useful in this type of problem [12, 14] since it allows the upper end of the eigenvalue spectrum of large sparse matrices to be extracted accurately without having to store the entire matrix in the computer's memory. Backbones of clusters built on lattices of $L = 70$, 100 and 150 were used to determine d_s^B and d_w^B. These were sufficiently large to contain enough data where the scaling relation can be tested (where λ is very close to 1) and small enough to get a large sample space of these clusters. Table 1 shows the number of samples taken for each value of L, along with the average number of sites in the average spanning cluster and its backbone used in each sample.

For all of the results in this paper, the random walker follows *blind ant* statistics. This means that on a simple cubic lattice with coordination number $z = 6$, the walker has a $\frac{1}{6}$ probability of moving to an adjoining occupied site, and a probability of $y/6$ of remaining in place, where y is the total number of blocked sites. All of the calculations took place on either a Kubota Pacific P-3000 mini-supercomputer or an IBM RS-6000 based machine.

3. Results and discussion

3.1. Estimation of d_f^B

The mass scaling is shown in figure 1, where a log–log plot of the mass of the backbone versus lattice size is given. For small L, there is a distinct upward curvature that is very

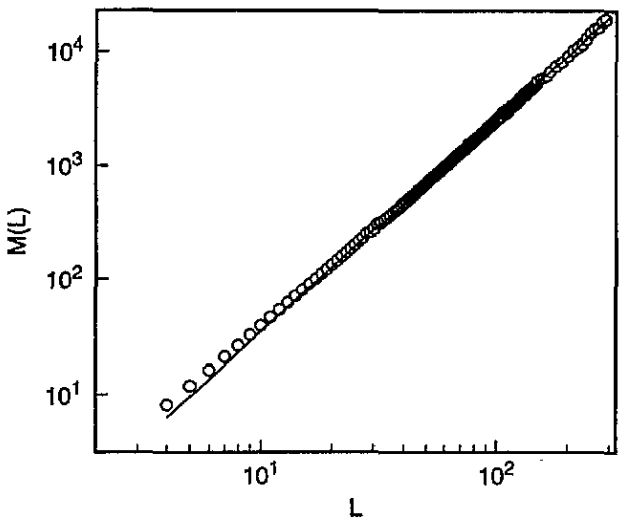

Figure 1. Plot of the mass of the backbone, $M(L)$ as a function of the lattice size L. The straight line is a fit to the points with $L \geqslant 40$.

easy to see when compared against the best-fit line for the points with $L \geqslant 40$. The slope of this line yields a $d_f^B = 1.855 \pm 0.015$.

In order to take into account the finite-size effects that were clearly present in figure 1, we assumed that the first-order correction to scaling was of the form

$$M \sim L^{d_f^B}(1 + \alpha L^{-\omega}). \tag{14}$$

If this is the form of the scaling, then the slope of the log–log plot in figure 1 should behave as

$$\frac{d \ln M}{d \ln L} \approx d_f^B - \alpha\omega L^{-\omega}. \tag{15}$$

To extract ω, we plotted the effective slope of graph of figure 1 versus $L^{-\omega}$, and found that the most linear plot resulted when ω was chosen as 1. This is consistent with previous correction to scaling results [26].

To show that the previous estimate for d_f^B is likely to be close to the asymptotic exponent, a plot of the effective slope of the data in figure 1 is shown in figure 2, plotted against $1/L$. For $L \leqslant 25$, the value of the effective exponent is the slope of a line formed by all of the points with a value of L less than or equal to that point. For $L > 25$, the effective exponent was calculated in a similar manner for each point, but instead of plotting all of the points, the average of each set of five points was taken, and that average value was plotted. This made the data visualization clearer and allowed us to calculate error bars which corresponded with the fluctuation in the data. For $L > 25$ the fluctuations in the values were much larger than the change in the average values, so we expect the error bars to correspond to the fluctuations and not from the actual spread in the data caused by binning different values of L.

The data acquired using the box-counting method on 100 randomly generated disorder configurations of size up to $L = 512$ are shown in figure 3 for various values of q. For $q = 0$, the box-counting method did not accurately measure the fractal dimension of the set. This was due to the fact that for $q = 0$, the information on the number of points in

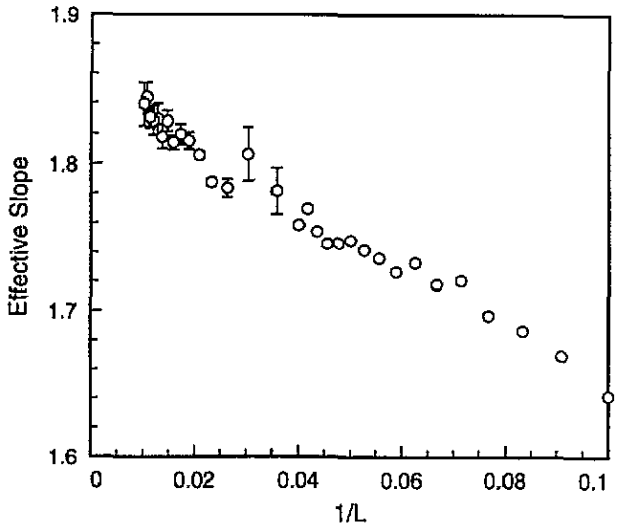

Figure 2. A plot of the effective slope of the previous graph of $M(L)$ versus $1/L$. The upward trend for larger L is clearly evident.

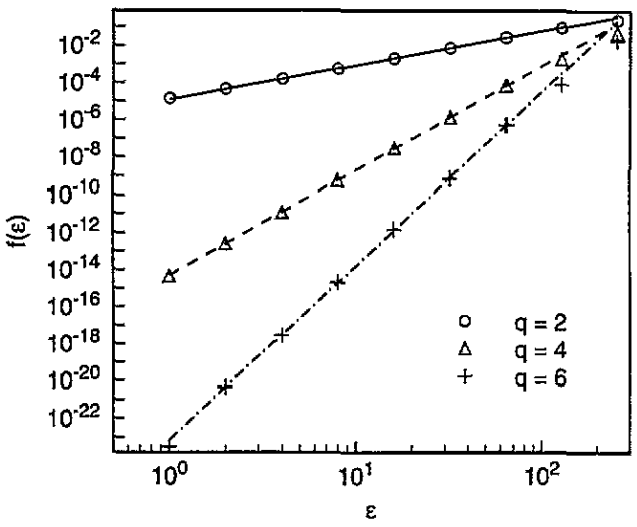

Figure 3. A log–log plot of $f(\epsilon) = \sum_{\nu=1}^{N(\epsilon)} [p_\nu(\epsilon)]^q$ versus the box size ϵ. The lines drawn through the points represent the best-fit line to the points where $2 \leqslant \epsilon \leqslant 128$.

each box was effectively lost. This is not always a problem when studying objects such as attractors in nonlinear dynamics which have continuous length scales, but can be when studying objects on a discrete grid which limits the possible number of box sizes. However, for $q \geqslant 2$, we obtained numbers that were always close to 1.86. Table 2 shows the effective fractal dimension for the different values of q. The box-counting method was not quite as precise as the mass-scaling method in this case, but it does provide a reasonable check of the results.

Table 2. Calculated values of $D_f(q)$ as a function of q.

q	0	1	2	4	6	8
$D_f(q)$	1.74 ± 0.03	1.85 ± 0.02	1.86 ± 0.01	1.87 ± 0.01	1.87 ± 0.01	1.865 ± 0.010

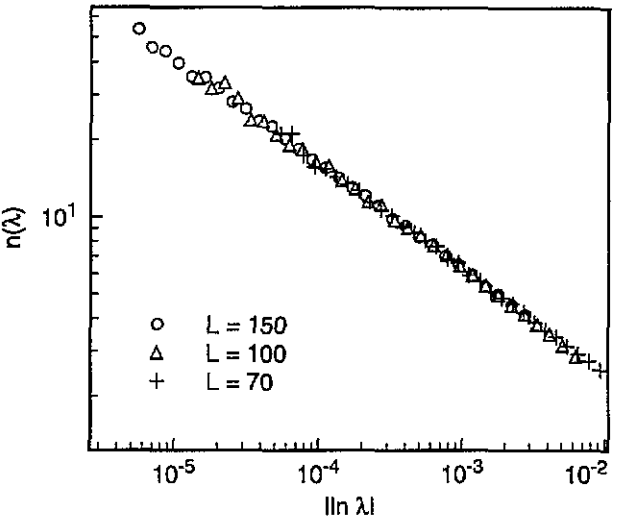

Figure 4. A plot of $n(\lambda)$ versus $|\ln\lambda|$ for $L = 150$ (○), 100 (△), and 70 (+).

3.2. Estimation of d_s^B and d_w^B.

The data shown in figure 4 is a collapsed log–log plot of $n(\lambda)$ versus $|\ln\lambda|$ for $L = 70$, 100 and 150. All of the data lie very close to a straight line, although there is a bit of structure to the points corresponding to λ very close to 1, and there is a slight decrease for some of the smaller eigenvalues for $L = 70$ as the data begin to leave the scaling region in which (7) is valid. A linear fit to these data (with the points which are not in the scaling region removed) yields a value of 0.410 ± 0.005. A fit to only the points in the $L = 150$ case gives a similar result. This corresponds to a value of $d_s^B = 1.18 \pm 0.01$. We believe this result is very accurate since it was not only obtained independently for different values of L, but smaller subsets of the data for each L were also analysed and separately found to have a similar slope.

Figure 5 shows the data for $\pi(\lambda)$ plotted against $|\ln\lambda|$ on a log–log scale. Again, the data follow a fairly straight line, but the fluctuations are more prominent in these data than they were for the $n(\lambda)$ data. Since most of the fluctuations seem to correspond to the similar but smaller fluctuations in the $n(\lambda)$ data, it turns out to be very useful to look at the quantity $\pi(\lambda)/n(\lambda)$. According to the scaling laws presented in section 1, this function should scale as

$$\pi(\lambda)/n(\lambda) \sim |\ln\lambda|^{2-d_s^B/2-2/d_w^B}. \tag{16}$$

A plot of this function for $L = 150$ is shown in figure 6. These data are much smoother, and one can see smaller details of the structure. The only part of the data deviating from a straight line is in the large-λ region, where they seem to decrease. A linear fit to the rest of the data gives a slope of 0.77 ± 0.01, which implies $d_w^B = 3.13 \pm 0.03$ (using the value of d_s^B calculated above).

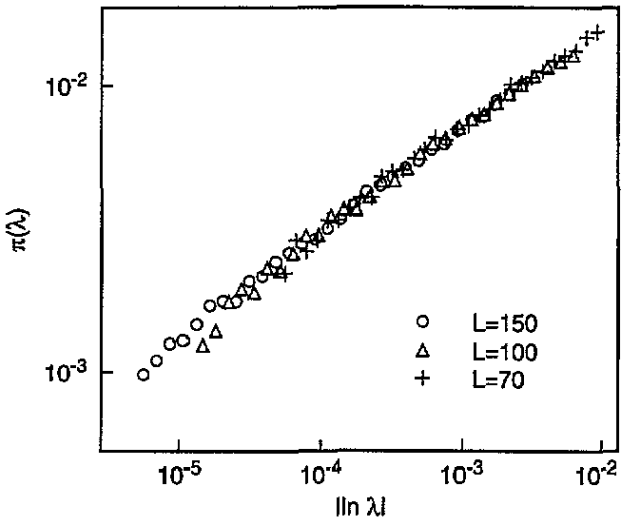

Figure 5. A plot of $\pi(\lambda)$ versus $|\ln\lambda|$ for $L = 150$ (○), 100 (△), and 70 (+).

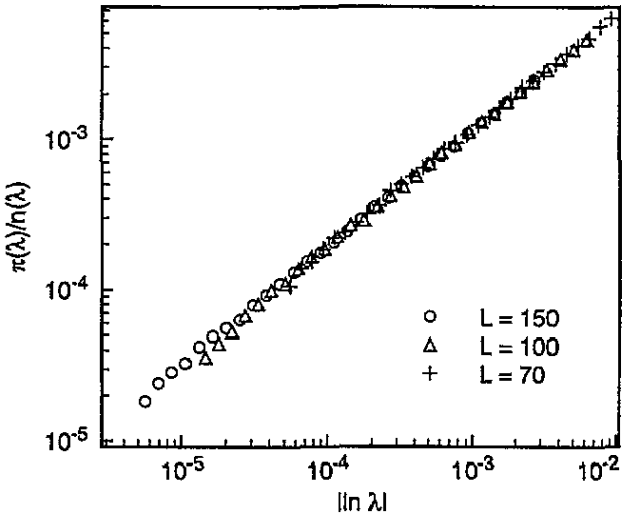

Figure 6. A plot of $n(\lambda)/\pi(\lambda)$ versus $|\ln\lambda|$ for $L = 150$ (○), 100 (△), and 70 (+).

The region of largest λ corresponds to long time-scales via the Laplace transform where $|\ln\lambda| \leftrightarrow t^{-1}$. Thus, the region excluded from the fit roughly corresponds to the time-scales $t > t_0$ where the corresponding length scale for diffusion is given by $\ell > \ell_0 \approx t_0^{d_w}$. Numerically, the crossover values occur in figure 6 where $|\ln\lambda| \approx 1 \times 10^{-4}$, 3×10^{-5} and 9×10^{-6} for $L = 70$, 100, and 150, respectively. In comparison, $(0.27 \times L)^{-d_w}$ gives 1×10^{-4}, 3.3×10^{-5}, and 9.3×10^{-6}. This suggests that the random walk is noticing the finite size of the cluster at length scales of approximately $L/4$. This is not an unreasonable length scale since the average is effectively over all walks in the cluster, and the finite nature of the backbone would be apparent much sooner than the finite size of the cluster.

3.3. Discussion of results

The estimate of d_f^B is significantly larger than previous estimates which used the same or similar methods. In [17] mass scaling of the backbone of incipient infinite clusters was done on cubic lattices of linear size L, where $6 \leqslant L \leqslant 40$. For this case they obtained a value of 1.77 ± 0.07 for d_f^B. Herrmann and Stanley [27] studied the distribution of the size of the 'blobs' which made up the backbone of incipient infinite clusters to determine that $d_f^B = 1.74 \pm 0.04$. However, these were also on relatively small clusters, with $4 \leqslant L \leqslant 60$. We believe that the reason our estimate is so much larger than previous estimates is that there is a significant unaccounted finite-size effect in their data. This can be easily inferred from our data in figure 2. When we use a subset of our data that corresponds to the data used in earlier works, we get results similar to the previous estimates. The value of d_f^B was also estimated by Hong and Stanley [28] using series-expansion techniques, and they obtained a value of 1.83 ± 0.08 in three dimensions.

We can now test (6) using the values we have estimated. From these values we get $2d_f^B/d_w^B = 1.182 \pm 0.015$, whereas our independent estimate of d_s^B is 1.18 ± 0.01. Unlike the results of [10] and [11], the scaling relation given by (6) appears to hold very well for the backbone.

Using equation (4) and the values determined above, one gets a value of 2.28 ± 0.03 for $\tilde{\mu}$. If one assumes that (6) is correct, then d_w^B can be written in terms of d_s^B and d_f^B, and the error in $\tilde{\mu}$ can be reduced even further. This result confirms the value of $\tilde{\mu}$ that has been estimated by a number of people very recently. In [30], finite-size scaling arguments are applied to direct conductance measurements of cubes with $2 \leqslant L \leqslant 80$ to obtain the value of $\tilde{\mu} = 2.276 \pm 0.012$. Our result is very close to this one, and if one considers the value of $\tilde{\mu}$ in [30] and our value of d_f^B to be independent quantities, then one obtains an even more precise value of $d_w^B = 3.126 \pm 0.015$. One can also calculate $\tilde{\mu}$ from Grassberger's [31] precise estimate of $\beta/\nu = 0.474 \pm 0.006$. This is done by using (3) and calculating d_w from the formula

$$d_w k = 1 - \beta/2\nu \tag{17}$$

where $k = 0.200 \pm 0.002$ [32]. Using these numbers, one gets a value of $\tilde{\mu} = 2.29 \pm 0.04$. The consistency of all of these values seems to strongly imply that the value of $\tilde{\mu}$ is very near the value we get using the direct estimates of d_w^B and d_f^B as given above.

4. Conclusions

We believe that the values estimated independently here for d_f^B, d_s^B and d_w^B (shown in table 3) represent a significantly improved accuracy over previous estimates for the three-dimensional critical percolating backbone. The value for d_f^B was calculated by simple but large-scale mass-scaling techniques and confirmed by box-counting. These exponent estimates are both consistent with the Alexander–Orbach scaling relation $d_s^B = 2d_f^B/d_w^B$ as applied to the backbone, and with previous results for related exponents on the full cluster. The Arnoldi–Saad method described in [14] proved to be an effective algorithm for this type of problem which involved calculating the largest eigenvalues of a very large sparse matrix.

Table 3. Values of critical exponents for the the three-dimensional percolating backbone.

d_f^B	1.855 ± 0.015
d_w^B	3.13 ± 0.03
d_s^B	1.18 ± 0.01

Acknowledgment

We would like to gratefully acknowledge the help of Sonali Mukherjee for fruitful discussions on the Arnoldi–Saad algorithm and on many aspects of diffusion.

References

[1] Feng S and Sen P 1984 *Phys. Rev. Lett.* **52** 216
[2] Kantor Y and Webman I 1984 *Phys. Rev. Lett.* **52** 1891
[3] Stanley H and Coniglio A 1984 *Phys. Rev.* B **29** 522
[4] Skal A and Shlovski B 1975 *Sov. Phys. Semicond.* **8** 1029
[5] de Gennes P 1976 *J. Physique Lett.* **37** L1
[6] Duering E and Bergman D 1989 *Physica* **157A** 125
[7] Nakanishi H *et al* 1993 *J. Physique I* **3** 733
[8] Gefen Y, A Aharony and S Alexander 1983 *Phys. Rev. Lett.* **50** 77
[9] Alexander S and Orbach R 1982 *J. Physique Lett.* **43** L625
[10] Dhar D and Ramaswamy R 1985 *Phys. Rev. Lett.* **54** 1346
[11] Nakanishi H and Herrmann H 1993 *J. Phys. A: Math. Gen.* **26** 4513
[12] Nakanishi H, Mukherjee S and Fuchs N H 1992 *Phys. Rev.* E **47** R1463
[13] Jacobs D and Nakanishi H 1990 *Phys. Rev.* A **41** 706
[14] Fuchs N and Nakanishi H 1991 *Phys. Rev.* A **43** 1721
[15] Rintoul M and Nakanishi H 1992 *J. Phys. A: Math. Gen.* **25** L945
[16] Tél T, Fülöp A and Vicsek T 1989 *Physica* **159A** 155
[17] Herrmann H, Hong D and Stanley H 1984 *J. Phys. A: Math. Gen.* **17** L261
[18] Puech L and Rammal R 1983 *J. Phys. C: Solid State Phys.* **16** L1197
[19] Hentschel H and Procaccia I 1983 *Physica* **8D** 435
[20] Grassberger P and Procaccia I 1984 *Physica* **13D** 34
[21] Block A, von Bloh W and Schellnhuber H 1990 *Phys. Rev.* A **42** 1869
[22] Meisel L, Johnson M and Cote P 1992 *Phys. Rev.* A **45** 6989
[23] Liebovitch L and Toth T 1989 *Phys. Lett.* **141A** 386
[24] Hou X, Gilmore R, Mindlin G and Solari H 1990 *Phys. Lett.* **151A** 43
[25] Arnoldi W 1951 *Q. Appl. Math.* **9** 17
[26] Stauffer D and Aharony A 1992 *Introduction to Percolation Theory* (Washington: Taylor and Francis)
[27] Herrmann H and Stanley H 1984 *Phys. Rev. Lett.* **53** 1121
[28] Hong D and Stanley H 1983 *J. Phys. A: Math. Gen.* **16** L475; 1984 *J. Phys. A: Math. Gen.* **17** 1121
[29] Saad Y 1980 *Linear Algebra Appl.* **34** 269
[30] Gingold D and Lobb C 1990 *Phys. Rev.* B **42** 8220
[31] Grassberger P 1992 *J. Phys. A: Math. Gen.* **25** 5867
[32] Duering E and Roman H 1991 *J. Stat. Phys.* **64** 851